Check for updates

Highly effective organic light-emitting diodes containing thermally activated delayed fluorescence emitters with horizontal molecular orientation†

Chan Hee Lee,[a] Shin Hyung Choi,[a] Sung Joon Oh,[a] Jun Hyeon Lee,[a] Jae Won Shim, [iD][b] Chihaya Adachi [iD][cd] and Sae Youn Lee [iD] *[a]

In this study, we report new thermally activated delayed fluorescence (TADF) emitters, **AcPYM** (10,10′-(pyrimidine-2,5-diylbis(4,1-phenylene))bis(9,9-dimethyl-9,10-dihydroacridine)) and **PxPYM** (10,10′-(pyrimidine-2,5-diylbis(4,1-phenylene))bis(10H-phenoxazine)), by employing donor units at the 2,5-positions of the pyrimidine acceptor unit. The donor–acceptor–donor (D–A–D) units combined in the linear molecular structure of **AcPYM** or **PxPYM** enhanced the horizontally oriented alignment, and the horizontal transition dipole moments were realized by up to 87% in the host matrix. Organic light-emitting diodes (OLEDs) containing **AcPYM** and **PxPYM** emitters realized external quantum efficiencies (η_{ext}) of 16.8% for blue and green emissions.

Introduction

After the first research into the organic light-emitting diodes (OLEDs) was reported in 1987,[1] significant improvements in OLEDs regarding efficiency, color purity, and lifetime have been achieved, leading to them becoming the next-generation light source for lighting and flexible display applications. Over the past several decades, various studies into organic emitters based on fluorescence and phosphorescence in the visible-light region have been conducted to improve the internal quantum efficiency (η_{int}).[2–7] Even though fluorescence emitters have outstanding reliability and stability, low exciton production efficiency ($\eta_{ST} = 25\%$) of fluorescence in electrical excitation limits the theoretical η_{int} to 25%. Phosphorescence emitters can achieve a theoretical η_{int} of nearly 100% from singlet (S_1) and triplet (T_1) exciton harvesting through intersystem crossing (ISC) between the S_1 and T_1 states using heavy transition metals.[8–12] However, phosphorescence emitters suffer from a strong exciton annihilation process and a drastic efficiency decrease under the high current density derived from the high density of T_1 excitons originating from their long radiative decay time (τ; μs–ms).[13]

Recently, a thermally activated delayed fluorescence (TADF) emitter that can substitute for fluorescence and phosphorescence emitters in OLEDs due to its effective S_1 and T_1 excitons harvesting by reverse ISC (RISC) from the T_1 to the S_1 state has been reported.[14–20] The up-conversion through RISC can only arise with a small S_1-to-T_1 state energy gap ($\Delta E_{ST} < 0.3$ eV) in TADF emitters, which is attained by providing less overlapping between the highest occupied molecular orbital (HOMO) and the lowest unoccupied molecular orbital (LUMO) levels. Furthermore, numerous studies have focused on molecular designs utilizing twisted molecular structures among the donor and acceptor units for reducing ΔE_{ST} and achieving efficient intramolecular charge transfer (ICT) based on pure organic derivatives.[21,22] Meanwhile, despite the development of various TADF emitters with η_{int} of nearly 100%, conventional OLEDs have a 20–25% external quantum efficiency (η_{ext}) limitation because of low light out-coupling efficiency (η_{out}).[23–25] External and internal optical modification of OLEDs such as attaching a microlens array, optimizing the layer thickness, and refractive index control of the internal layers have been widely studied to increase η_{out}.[26–38] Another promising approach for enhancing η_{out} is to introduce horizontally oriented emitters. Previous research by Yokoyama and co-workers demonstrated an increase of η_{out} in OLEDs by applying horizontally aligned emitters having horizontal transition dipole moment orientation on the substrate.[39–41] Furthermore, the orientation degree of the emitters can be controlled by the shape of the molecules: rod- or disk-like structures prefer high degrees of horizontal transition dipole moments for perpendicular light emission.

[a]*Department of Energy and Materials Engineering, Dongguk University, Seoul, 04620, Republic of Korea. E-mail: saeyounlee@dongguk.edu*

[b]*School of Electrical Engineering, Korea University, Seoul, 02841, South Korea*

[c]*Center for Organic Photonics and Electronics Research (OPERA), Kyushu University, 744 Motooka, Nishi-ku, Fukuoka, 819-0395, Japan*

[d]*Department of Chemistry and Biochemistry, Kyushu University, 744 Motooka, Nishi-ku, Fukuoka, 819-0395, Japan*

† Electronic supplementary information (ESI) available: For synthesis and characterization details of materials. See DOI: 10.1039/d0ra07865d

In this study, we developed two pyrimidine-based TADF emitters: 10,10′-(pyrimidine-2,5-diylbis(4,1-phenylene))bis(9,9-dimethyl-9,10-dihydroacridine) (**AcPYM**) and 10,10′-(pyrimidine-2,5-diylbis(4,1-phenylene))bis(10H-phenoxazine) (**PxPYM**) and adopted donor–acceptor–donor (D–A–D) combined linear molecular structures based on a combination of donor units of 9,9-dimethylacridin (Ac) or phenoxazine (Px) and one of the pyrimidine acceptor units. The donor units were introduced at the 2,5-position of the pyrimidine unit to compose a linear D–A–D framework of emitters to induce a horizontal transition dipole moment. These new emitters achieved small ΔE_{ST} due to less overlapping between the HOMO and LUMO levels and improved RISC through effective exciton harvesting. Furthermore, a high rate of horizontal molecular orientation of over 80% was observed in angle-dependent photoluminescence (PL) measurements of the host matrix. OLEDs employing horizontally oriented TADF emitters achieved high η_{ext} of 16.8% in blue and green light emissions.

Experimental

Materials

All reagents and solvents were prepared from Alfa Aesar, Sigma-Aldrich, and Tokyo Chemical Industry. Two intermediates, 9,9-dimethyl-10-(4-(4,4,5,5-tetramethyl-1,3,2-dioxaborolan-2-yl)phenyl)-9,10-dihydroacridine (**1**) and 10-(4-(4,4,5,5-tetramethyl-1,3,2-dioxaborolan-2-yl)phenyl)-10H-phenoxazine (**2**), were synthesized as reported previously.[42]

Synthesis

Synthesis of AcPYM. 5-Bromo-2-chloropyrimidine (0.50 g, 2.58 mmol) and **1** (2.34 g, 5.69 mmol) were dissolved in 1,4-dioxane (30 mL) under an N_2 atmosphere. Next, sodium carbonate (2.4 M, 15 mL) and tetrakis(triphenylphosphine)-palladium(0) (0.24 g, 0.21 mmol) were added and the mixture refluxed for 12 h. After cooling down to room temperature, the solution was poured into chloroform and distilled water for extraction. The chloroform layer was washed with distilled water several times and dried over magnesium sulfate ($MgSO_4$). The crude product was filtered by using Celite 545 and purified via column chromatography on silica gel (eluent: dichloromethane/hexane, 4 : 1 v/v). The product was dried in a vacuum oven to give a white powder (yield = 1.03 g; 62%) and further purified via vacuum train sublimation. ^{1}H NMR (500 MHz, CDCl₃): δ 9.20 (s, 2H), 8.79 (d, J = 8.5 Hz, 2H), 7.95 (d, J = 8.5 Hz, 2H), 7.55 (d, J = 8.0 Hz, 4H), 7.49 (t, J = 6.5 Hz, 4H), 7.03–6.93 (m, 8H), 6.38 (d, J = 8.0 Hz, 2H), 6.35 (d, J = 8.0 Hz, 2H). ^{13}C NMR (500 MHz, CDCl₃) data are as follows: 155.43, 143.86, 140.73, 132.56, 131.66, 130.82, 130.24, 129.28, 126.44, 125.39, 120.87, 120.73, 36.04, 31.30; Anal. calcd (%) for $C_{46}H_{38}N_4$: C 85.42; H 5.92; N 8.66; found: C 85.32; H 5.92; N 8.68.

Synthesis of PxPYM. The synthesis of this compound was similar to **AcPYM** using **2** (3.07 g; 7.96 mmol). The product was dried in vacuum oven to give a yellow powder (yield = 1.30 g; 60%) and further purified by vacuum train sublimation. ^{1}H NMR (500 MHz, CDCl₃): δ 9.14 (s, 2H), 8.74 (d, J = 8 Hz, 2H),

7.90 (d, J = 8.0 Hz, 2H), 7.56 (d, J = 8.5 Hz, 2H), 7.53 (d, J = 8.5 Hz, 2H), 6.74–6.60 (m, 12H), 6.05 (dd, J = 6.5, 1.5 Hz, 2H), 6.02 (dd, J = 6.0, 1.5 Hz, 2H). ^{13}C NMR (500 MHz, CDCl₃) data are as follows: 206.91, 155.40, 144.03, 134.10, 132.10, 131.14, 130.97, 129.47, 123.30, 121.69, 121.53, 115.67, 115.56, 113.38, 113.28, 110.73, 110.41, 31.24, 30.92; Anal. calcd (%) for $C_{40}H_{26}N_4$: C 80.79; H 9.42; N 4.41; found: C 80.91; H 9.47; N 4.26.

Results and discussion

Synthesis and thermal properties

AcPYM and **PxPYM** were synthesized through Suzuki coupling reactions with either Ac or Px, respectively, with the bromine-substituted pyrimidine (Scheme 1).[42] The chemical structures of the newly synthesized emitters were analyzed using ^{1}H and ^{13}C NMR spectroscopy, MALDI-TOF mass spectrometry, and elemental analysis. In addition, Differential Scanning Calorimetry (DSC) and thermogravimetric analysis (TGA) was performed to analyze the thermal properties of the emitters (Fig. S4 and S5†); it was observed that the decomposition temperatures (T_d) of **AcPYM** and **PxPYM** were 435 and 463 °C, respectively.

Density functional theory (DFT) calculations

The optimized molecular structures, excited states energy levels, and frontier molecular orbital contributions of **AcPYM** and **PxPYM** were calculated via a time-dependent DFT (TD-DFT) at the B3LYP/6-31G(d,p) level (Fig. 1). These emitters have dihedral angles between the phenyl linkers and the Ac or Px units ($\theta_{D-\pi}$) of 89.5–89.8° and 87.8–89.3° for **AcPYM** and **PxPYM**, respectively. Moreover, the LUMO and HOMO levels of **AcPYM** and **PxPYM** are localized on the pyrimidine acceptor and either the Ac or Px donor units, respectively. This good separation of the frontier molecular orbital distributions of **AcPYM** and **PxPYM** originating from the highly sterically hindered structure contributed to the relatively small calculated ΔE_{ST} of 0.01 eV.

Photophysical properties

Fig. 2 displays spectra of the ultraviolet-visible (UV-Vis) absorbance and the PL of the emitters in toluene. The broad 375 and 394 nm-centered absorption peaks and the 477 and 532 nm-centered blue and green PL emission peaks (λ_{PL}) of **AcPYM**
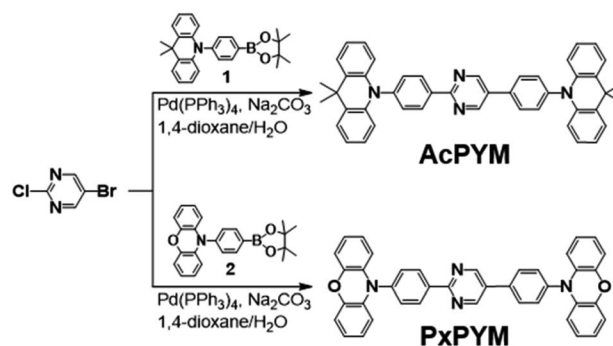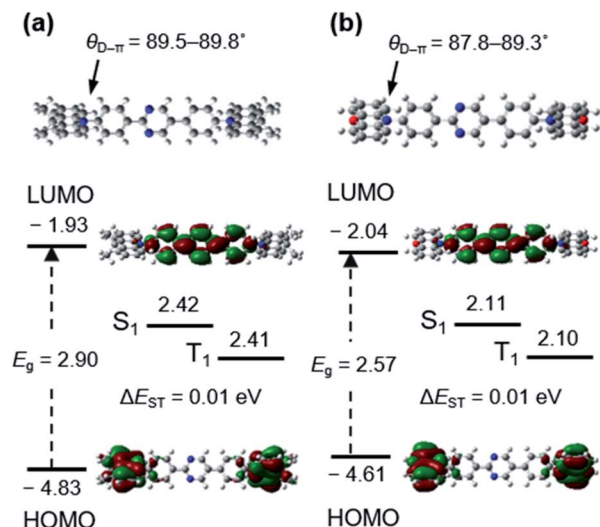

Scheme 1 Synthesis of **AcPYM** and **PxPYM**.

Fig. 1 The optimized molecular structure, singlet (S_1) and triplet (T_1) energy levels, and HOMO and LUMO distribution of (a) AcPYM and (b) PxPYM calculated via DFT and TD-DFT at the B3LYP/6-31G(d,p) level.
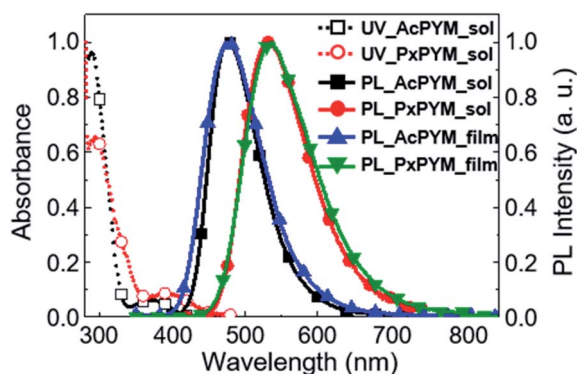

Fig. 2 UV-Vis absorbance and PL spectra of AcPYM and PxPYM in toluene, and 6 wt% AcPYM and PxPYM:PPT-doped films.

Fig. 3 Transient decay curves of the (a) 6 wt% AcPYM:PPT- and (b) 6 wt% PxPYM:PPT-doped films (inset: time-resolved PL spectra and streak images).

Fig. 4 Angle-dependent PL spectra of AcPYM and PxPYM (p-polarized light from 15 nm thin film at 480 nm for AcPYM and 525 nm for PxPYM). Θ is an anisotropy factor calculated from the fitted solid lines, while the symbols present the experimental data.

and PxPYM were observed in the UV-Vis and PL spectra under photoexcitation of oxygen-free toluene, respectively. Furthermore, 6 wt% AcPYM and PxPYM doped in 2,8-bis(diphenylphosphoryl)-dibenzo[b,d]thiophene (PPT) host thin films were prepared to confirm the photophysical properties of the emitters in the solid-state. Because of the higher T_1 energy level of PPT (E_T = 3.1 eV) compare with AcPYM and PxPYM (E_T = 2.65 and 2.58 eV, Fig. S7†), the PPT host was chosen to contain the reverse energy transfer between the emitter and the host.[17,19,43] As shown in Fig. 2, the 6 wt% AcPYM:PPT-doped film exhibited blue emission with 478 nm λ_{PL}, while the 6 wt% PxPYM:PPT-doped film emitted green light at around 537 nm.

The PL quantum yields (PLQY, Φ_{PL}) of the 6 wt% AcPYM- and PxPYM-doped films in PPT hosts were measured using an integrating sphere, with which Φ_{PL} levels of 53.3% and 78.0% were observed. We also examined temperature-dependent transient PL decays to identify the TADF characteristics of the emitt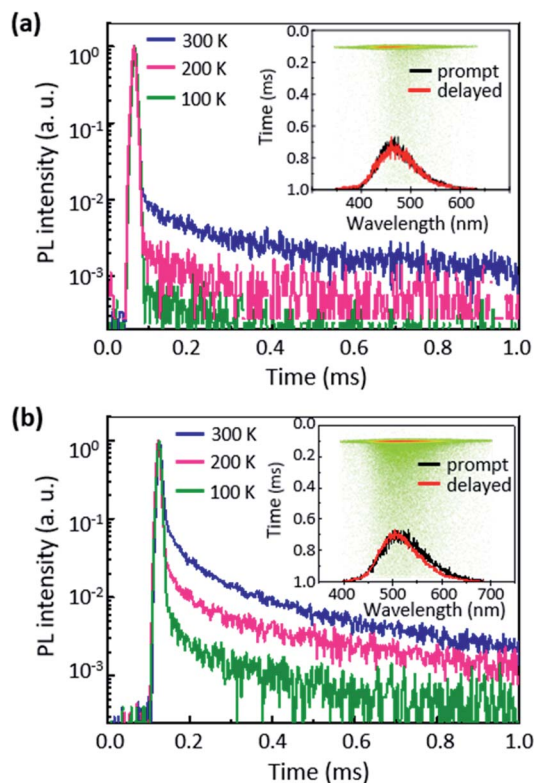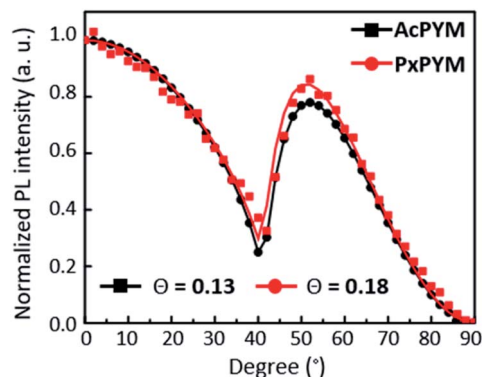ers' temperature range from 100 to 300 K using a streak camera (Fig. 3). The delayed component PL intensity increased while the temperature raise from 100 to 300 K, thereby demonstrating that the thermal energy at high temperature accelerated the RISC process.[31] Furthermore, 19 and 17 ns of the prompt fluorescence lifetimes (τ_p) and 486 and 287 μs of the delayed fluorescence lifetimes (τ_d) were observed in the double-exponential function fitted transient PL decay curves of AcPYM and PxPYM, respectively. Φ_{PL} and the ISC and RISC rate constants are summarized in Table S3.†[44]
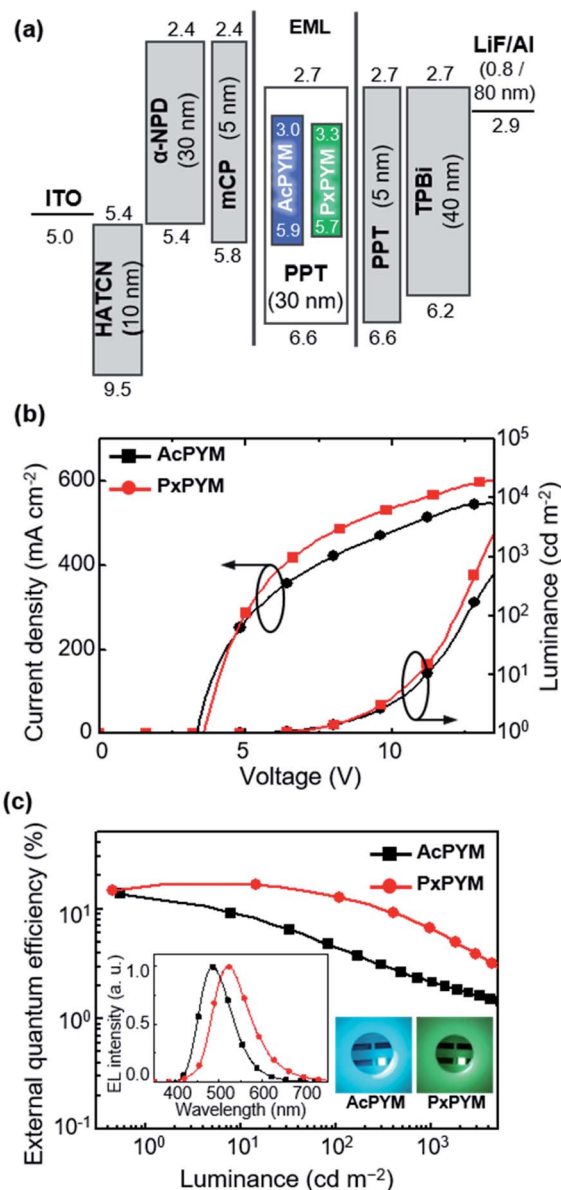
Fig. 5 (a) Energy level diagrams, (b) current density–voltage–luminance (J–V–L) curves, and (c) external quantum efficiency (η_{ext}) versus luminance plots of the devices employing AcPYM or PxPYM (inset: EL spectra at 10 mA cm^{-2} and light-emitting images under electrical excitation).

The horizontal alignment of the emitters was confirmed via angle-dependent PL measurements (Fig. 4). To verify the molecular orientation of the AcPYM and PxPYM, the angle dependence of the PL intensity of emitters in the host matrix

was estimated to fit the experimental data. Moreover, the horizontal molecular orientation degree was estimated using anisotropy factor Θ calculated from the perpendicularly oriented fraction to the total amount of transition dipole moments:[30,39,45]

$$\Theta = [p_z]/([p_x] + [p_y] + [p_z])$$

where $[p_z]$ is vertical, and $[p_x]$ and $[p_y]$ are horizontal transition dipole moments. A Θ value of 1/3 means complete isotropy ($[p_x] = [p_y] = [p_z] = 1$), and the value of zero means perfectly horizontal ($[p_x] = [p_y] = 1$, $[p_z] = 0$). From the experimental results, Θ was equal to 0.13 and 0.18 for AcPYM and PxPYM:PPT-doped films, respectively, demonstrating that the AcPYM:PPT-doped film has 87% horizontal transition dipole moments and the PxPYM:PPT-doped film has 83%. Moreover, the values are higher than those of previously reported emitters having random molecular orientation, indicating that the devices developed using AcPYM and PxPYM emitters showed higher η_{ext} values.

Electroluminescence (EL) performance

The EL characteristics of TADF-OLEDs using AcPYM and PxPYM emitters in devices of indium tin oxide (ITO)/1,4,5,7,8,11-hexaazatriphenylene-hexacarbonitrile (HATCN, 10 nm)/4,4′-bis[N-(1-naphtyl)-N-phenylamino]-1,1′-biphenyl (α-NPD, 30 nm)/1,3-bis(9-carbazolyl)benzene (mCP, 5 nm)/6 wt% emitter: PPT (30 nm)/PPT (5 nm)/1,3,5-tris(N-phenylbenzimidazol-2-yl)benzene (TPBi, 40 nm)/lithium fluoride (LiF, 0.8 nm)/aluminum (Al, 80 nm) (Fig. 5(a)). To prevent triplet exciton quenching from emitting layer (EML) to hole- and electron-transporting layer in these devices, 5 nm thin layers of mCP and PPT having high T_1 energy levels (2.9 and 3.1 eV, respectively) were added as the neighboring layers of the EML.

The current density–voltage–luminance (J–V–L) properties are displayed in Fig. 5(b). The TADF-OLEDs employing AcPYM and PxPYM as emitters exhibited blue and green EL emission peaks (λ_{EL}) at 487 and 524 nm, respectively (Fig. 5(c)). In addition, below a turn-on voltage of 3.6 V for all devices exhibited maximum luminance (L_{max}) values of 20 370 cd m^{-2} for AcPYM and 19 390 cd m^{-2} for PxPYM. The AcPYM-based TADF-OLEDs achieved η_{ext} of 11.9%, current efficiency (η_c) of 27.0 cd A^{-1}, and power efficiency (η_p) of 25.0 lm W^{-1}, while the PxPYM-based OLEDs achieved 16.8%, 52.2 cd A^{-1}, and 41.0 lm W^{-1}, respectively (Table 1).

Conclusions

We designed and synthesized linear D–A–D-structured TADF emitters AcPYM and PxPYM with Ac or Px donor units,

Table 1 EL performances of the devices using AcPYM or PxPYM as the emitter

Emitter	λ_{EL}[a] (nm)	$V_{turn-on}$[b] (V)	L_{max}[c] (cd m^{-2})	η_c[d] (cd A^{-1})	η_p[e] (lm W^{-1})	η_{ext}[f] (%)	CIE (x,y)[g]
AcPYM	487	3.4	20 370	27.0	25.0	11.9 (@3.4 V)	(0.17, 0.32)
PxPYM	524	3.6	19 390	52.2	41.0	16.8 (@4.0 V)	(0.29, 0.51)

[a] The peak wavelength of EL emission. [b] Turn-on voltage at 1 cd m^{-2}. [c] maximum luminance. [d] Maximum current efficiency. [e] Maximum power efficiency. [f] External quantum efficiency. [g] Commission Internationale de l'Éclairage (CIE) color coordination.

respectively, at the 2,5-positions of the pyrimidine acceptor unit. These newly designed TADF emitters realized a small ΔE_{ST}, which accelerated the RISC and increased the exciton harvesting efficiency. Moreover, the molecular orientation of the emitters was estimated by angle-dependent PL measurements, indicating that both **AcPYM** and **PxPYM** had high rates of horizontal molecular alignment (87% and 83%, respectively). The TADF-OLEDs fabricated using either **AcPYM** or **PxPYM** as the emitter exhibited η_{ext} values of 11.9% and 16.8%, respectively, both of which exceed the theoretical η_{ext} evaluated for a random distribution of emitting dipoles. We also believe that our approach clearly presents a move toward horizontally oriented TADF emitters that will inspire the realization of highly effective TADF-OLEDs in the future.

Conflicts of interest

There are no conflicts to declare.

Acknowledgements

Notes and references

1 C. W. Tang and S. A. VanSlyke, *Appl. Phys. Lett.*, 1987, **51**, 913.
2 F. B. Dias, K. N. Bourdakos, V. Jankus, K. C. Moss, K. T. Kamatekar, V. Bhalla, J. Santos, M. R. Bryce and A. P. Monkman, *Adv. Mater.*, 2013, **25**, 3707.
3 G. Schwartz, M. Pfeiffer, S. Reineke, K. Walzer and K. Leo, *Adv. Mater.*, 2007, **19**, 3672.
4 Q. Wang, J. Ding, D. Ma, Y. Cheng, L. Wang, X. Jing and F. Wang, *Adv. Funct. Mater.*, 2009, **19**, 84.
5 Y. Sun, N. C. Giebink, H. Kanno, B. Ma, M. E. Thompson and S. R. Forrest, *Nature*, 2006, **440**, 908.
6 M. A. Baldo, D. F. O'Brien, Y. You, A. Shoustikov, S. Sibley, M. E. Thompson and S. R. Forrest, *Nature*, 1998, **395**, 151.
7 C. Adachi, M. A. Baldo and S. R. Forrest, *J. Appl. Phys.*, 2000, **87**, 8049.
8 J. Tagare and S. Vaidyanathan, *J. Mater. Chem. C*, 2018, **38**, 10138.
9 I. S. Park, H. Komiyama and T. Yasuda, *Chem. Sci.*, 2017, **8**, 953.
10 H. V. R. Dias, H. V. K. Diyabalanage, M. A. Rawashdeh-Omary, M. A. Franzman and M. A. Omary, *J. Am. Chem. Soc.*, 2003, **125**, 12072.
11 A. B. Tamayo, B. D. Alleyne, P. I. Djurovich, S. Lamansky, I. Tsyba, N. N. Ho, R. Bau and M. E. Thompson, *J. Am. Chem. Soc.*, 2003, **125**, 7377.
12 W. Sotoyama, T. Satoh, N. Sawatari and H. Inoue, *Appl. Phys. Lett.*, 2005, **86**, 153505.
13 S. Reineke, K. Walzer and K. Leo, *Phys. Rev. B: Condens. Matter Mater. Phys.*, 2007, **75**, 125328.
14 S. H. Choi, C. H. Lee, C. Adachi and S. Y. Lee, *Dyes Pigm.*, 2019, **171**, 107775.
15 H. Uoyama, K. Goushi, K. Shizu, H. Nomura and C. Adachi, *Nature*, 2012, **492**, 234.
16 Q. Zhang, B. Li, S. Huang, H. Nomura, H. Tanaka and C. Adachi, *Nat. Photonics*, 2014, **8**, 326–332.
17 S. Y. Lee, T. Yasuda, H. Nomura and C. Adachi, *Appl. Phys. Lett.*, 2012, **101**, 093306.
18 C. Adachi, *Jpn. J. Appl. Phys.*, 2014, **53**, 060101.
19 S. H. Choi, C. H. Lee, C. Adachi and S. Y. Lee, *Dyes Pigm.*, 2020, **172**, 107849.
20 S. Hirata, Y. Sakai, K. Masui, H. Tanaka, S. Y. Lee, H. Nomura, N. Nakamura, M. Yasumatsu, H. Nakanotani, Q. Zhang, K. Shizu, H. Miyazaki and C. Adachi, *Nat. Mater.*, 2015, **14**, 330.
21 X. Lv, R. Huang, S. Sun, Q. Zhang, S. Xiang, S. Ye, P. Leng, F. B. Dias and L. Wang, *ACS Appl. Mater. Interfaces*, 2019, **11**, 10758.
22 F. Baraket, B. Pedras, É. Torres, M. J. Brites, M. Dammak and M. N. Berberan-Santos, *Dyes Pigm.*, 2020, **175**, 108114.
23 G. Méhes, H. Nomura, Q. Zhang, T. Nakagawa and C. Adachi, *Angew. Chem., Int. Ed.*, 2012, **51**, 11311.
24 S. Möller and S. R. Forrest, *J. Appl. Phys.*, 2002, **91**, 3324.
25 K. Hong, H. K. Yu, I. Lee, K. Kim, S. Kim and J. L. Lee, *Adv. Mater.*, 2010, **22**, 4890.
26 S. Reineke, F. Lindner, G. Schwartz, N. Seidler, K. Walzer, B. Lüssem and K. Leo, *Nature*, 2009, **459**, 234.
27 Y. Sun and S. R. Forrest, *Nat. Photonics*, 2008, **2**, 483.
28 K. B. Choi, S. J. Shin, T. H. Park, H. J. Lee, J. H. Hwang, J. H. Park, B. Y. Hwang, Y. W. Park and B. K. Ju, *Org. Electron.*, 2014, **15**, 111.
29 M. G. Helander, Z. B. Wang, J. Qiu, M. T. Greiner, D. P. Puzzo, Z. W. Liu and Z. H. Lu, *Science*, 2011, **332**, 944.
30 C. Mayr, S. Y. Lee, T. D. Schmidt, T. Yasuda, C. Adachi and W. Brütting, *Adv. Funct. Mater.*, 2014, **24**, 5232.
31 T. A. Lin, T. Chatterjee, W. L. Tsai, W. K. Lee, M. J. Wu, M. Jiao, K. C. Pan, C. L. Yi, C. L. Chung, K. T. Wong and C. C. Wu, *Adv. Mater.*, 2016, **28**, 6976.
32 Y. S. Park, S. Lee, K. H. Kim, S. Y. Kim, J. H. Lee and J. J. Kim, *Adv. Funct. Mater.*, 2013, **23**, 4914.
33 K. H. Kim, E. S. Ahn, J. S. Huh, Y. H. Kim and J. J. Kim, *Chem. Mater.*, 2016, **28**, 7505.
34 K. H. Kim, J. L. Liao, S. W. Lee, B. Sim, C. K. Moon, G. H. Lee, H. J. Kim, Y. Chi and J. J. Kim, *Adv. Mater.*, 2016, **28**, 2526.
35 K. H. Kim, J. Y. Baek, C. W. Cheon, C. K. Moon, B. Sim, M. Y. Choi, J. J. Kim and Y. H. Kim, *Chem. Commun.*, 2016, **52**, 10956.
36 C. S. Oh, C. K. Moon, J. M. Choi, J. S. Huh, J. J. Kim and J. Y. Lee, *Org. Electron.*, 2017, **42**, 337.
37 P. Rajamalli, N. Senthikumar, P. Y. Huang, C. C. Ren-Wu, H. W. Lin and C. H. Cheng, *J. Am. Chem. Soc.*, 2017, **139**, 10948.

38 S. J. Woo, Y. Kim, M. J. Kim, J. Y. Baek, S. K. Kwon, Y. H. Kim and J. J. Kim, *Chem. Mater.*, 2018, **30**, 857.

39 D. Yokoyama, A. Sakaguchi, M. Suzuki and C. Adachi, *Org. Electron.*, 2009, **10**, 127.

40 D. Yokoyama, *J. Mater. Chem.*, 2011, **21**, 19187.

41 Y. Sakai, M. Shibata and D. Yokoyama, *Appl. Phys. Express*, 2015, **8**, 096601.

42 S. Y. Lee, T. Yasuda, I. S. Park and C. Adachi, *Dalton Trans.*, 2015, **44**, 8356.

43 Y. S. Tsai, L. A. Hong, F. S. Juang and C. Y. Chen, *J. Lumin.*, 2014, **153**, 312.

44 K. Goushi, K. Yoshida, K. Sato and C. Adachi, *Nat. Photonics*, 2012, **6**, 253.

45 T. D. Schmidt, D. S. Setz, M. Flämmich, J. Frischeisen, D. Michaelis, B. C. Krummacher, N. Danz and W. Brütting, *Appl. Phys. Lett.*, 2011, **99**, 163302.